NASA/TM—2015-218847

Mechanical Properties of a High Lead Glass Used in the Mars Organic Molecule Analyzer

Jonathan A. Salem
Glenn Research Center, Cleveland, Ohio

Nathan A. Smith
Millennium Engineering and Integration Company, Arlington, Virginia

Akif Ersahin
MAE Aerospace, Woodbridge, Connecticut

August 2015

NASA STI Program . . . in Profile

Since its founding, NASA has been dedicated to the advancement of aeronautics and space science. The NASA Scientific and Technical Information (STI) Program plays a key part in helping NASA maintain this important role.

The NASA STI Program operates under the auspices of the Agency Chief Information Officer. It collects, organizes, provides for archiving, and disseminates NASA's STI. The NASA STI Program provides access to the NASA Technical Report Server—Registered (NTRS Reg) and NASA Technical Report Server—Public (NTRS) thus providing one of the largest collections of aeronautical and space science STI in the world. Results are published in both non-NASA channels and by NASA in the NASA STI Report Series, which includes the following report types:

- TECHNICAL PUBLICATION. Reports of completed research or a major significant phase of research that present the results of NASA programs and include extensive data or theoretical analysis. Includes compilations of significant scientific and technical data and information deemed to be of continuing reference value. NASA counter-part of peer-reviewed formal professional papers, but has less stringent limitations on manuscript length and extent of graphic presentations.

- TECHNICAL MEMORANDUM. Scientific and technical findings that are preliminary or of specialized interest, e.g., "quick-release" reports, working papers, and bibliographies that contain minimal annotation. Does not contain extensive analysis.

- CONTRACTOR REPORT. Scientific and technical findings by NASA-sponsored contractors and grantees.

- CONFERENCE PUBLICATION. Collected papers from scientific and technical conferences, symposia, seminars, or other meetings sponsored or co-sponsored by NASA.

- SPECIAL PUBLICATION. Scientific, technical, or historical information from NASA programs, projects, and missions, often concerned with subjects having substantial public interest.

- TECHNICAL TRANSLATION. English-language translations of foreign scientific and technical material pertinent to NASA's mission.

For more information about the NASA STI program, see the following:

- Access the NASA STI program home page at http://www.sti.nasa.gov

- E-mail your question to help@sti.nasa.gov

- Fax your question to the NASA STI Information Desk at 757-864-6500

- Telephone the NASA STI Information Desk at 757-864-9658

- Write to:
  NASA STI Program
  Mail Stop 148
  NASA Langley Research Center
  Hampton, VA 23681-2199

NASA/TM—2015-218847

Mechanical Properties of a High Lead Glass Used in the Mars Organic Molecule Analyzer

Jonathan A. Salem
Glenn Research Center, Cleveland, Ohio

Nathan A. Smith
Millennium Engineering and Integration Company, Arlington, Virginia

Akif Ersahin
MAE Aerospace, Woodbridge, Connecticut

National Aeronautics and
Space Administration

Glenn Research Center
Cleveland, Ohio 44135

August 2015

Acknowledgments

Thanks to Chris Burke for machining test fixtures and to George Quinn for useful discussions.

Level of Review: This material has been technically reviewed by technical management.

Available from

NASA STI Program
Mail Stop 148
NASA Langley Research Center
Hampton, VA 23681-2199

National Technical Information Service
5285 Port Royal Road
Springfield, VA 22161
703-605-6000

This report is available in electronic form at http://www.sti.nasa.gov/ and http://ntrs.nasa.gov/

Mechanical Properties of a High Lead Glass Used in the Mars Organic Molecule Analyzer

Jonathan A. Salem
National Aeronautics and Space Administration
Glenn Research Center
Cleveland, Ohio 44135

Nathan A. Smith
Millennium Engineering and Integration Company
Arlington, Virginia 22202

Akif Ersahin
MAE Aerospace
Woodbridge, Connecticut 06525

Abstract

The elastic constants, strength, fracture toughness, slow crack growth parameters, and mirror constant of a high lead glass supplied as tubes and funnels were measured using ASTM International (formerly ASTM, American Society for Testing and Materials) methods and modifications thereof. The material exhibits lower Young's modulus and slow crack growth exponent as compared to soda-lime silica glass. Highly modified glasses exhibit lower fracture toughness and slow crack growth exponent than high purity glasses such as fused silica.

Introduction

The Exobiology on Mars program is a series of European Space Agency missions to understand if life ever existed on Mars. NASA is contributing scientific, engineering, and technical expertise to international efforts to explore the Red Planet. NASA's participation in the 2018 Exobiology on Mars Rover mission includes providing critical elements to the premier chemical analysis instrument on the rover, the Mars Organic Molecule Analyzer (MOMA). Some of the MOMA components are very brittle and require reliability analysis. This report provides results of mechanical testing and fractography of a high lead glass used in the MOMA system.

Test Materials

The test material was readily available as system subcomponents in the geometry of tubes and funnels with a curved spout. The cross section of the tubes, shown in Figure 1, consisted of six trapezoidal cavities arranged to form a central hexagon. Various regions of the tubes and funnel were either abraded, unabraded or metallized, thereby creating multiple surface finishes and flaw populations. Elastic modulus and strength tests were perform with the tubes, whereas slow crack growth and inert strength tests were performed with the funnels. With the exception of the test geometries, the tests nominally conformed to ASTM International standards C1289, C1368, and C1421.

Mechanical Properties

Elastic Modulus

The elastic modulus was measured using impulse excitation in accordance with ASTM International C1259 with the exception of the previously described cross section. In order to account for the influence of cross section, the differences in inertia and density as determined via finite element analysis (FEA) were used in the calculations. The measured Young's modulus is E = 58.5±0.6 GPa, which is much lower than that of soda-lime silicate, but comparable to that of other high lead glasses (Refs. 1 and 2). Figure 2 shows the results as a function of bulk density. Because of the different sections of the specimens, it is likely that the apparent variation in bulk density is a result of geometric effects rather than real material density variation.

Fracture Strength

The fracture strength, S_f, was measured in four-point bending with 10 and 20 mm spans. The strength was calculated from

$$S_f = \frac{Mc}{I} \tag{1}$$

where M is the applied moment, c is the distance to the surface from the neutral axis, and I is the moment of inertia of the cross section as estimated with FEA. The resultant Weibull parameters are summarized in Table 1 and plots are show in Figures 3 and 4 for all of the data and the data censored into groups by fracture location: in the abraded region, the metallized region, or the unabraded region. Failure typically occurred in the abraded region and the Weibull statistics are similar for all fracture locations. Although the Weibull distribution provides an adequate fit, the log normal distribution provides a better fit, Figure 5.

Fracture Mirror Constants

The fracture mirror radii associated with the mist and hackle regions were measured on thirty of the strength specimens. Figures 6 to 9 show example fracture surfaces, which were frequently asymmetric. Fracture was the result of surface damage, shown in Figure 10, in the form of scratches, checks, and gouges. Because the strengths were narrowly distributed, the mirror constants were estimated point wise from, rather than by curve fitting of, the function

$$S_f = \frac{A_i}{\sqrt{r_i}} \tag{2}$$

where A_i is the particular boundary constant and r_i is the corresponding boundary radius. The resultant mirror-mist and mist-hackle constants were A_M = 1.4±0.1 and A_H = 1.6±0.1 MPa√m.

Fracture Toughness

Fracture toughness was estimated from the size of the failure origins on fracture strength specimens exhibiting relatively symmetric mirror patterns along with the Newman-Raju equations (Ref. 3). Use of a stress intensity factor coefficient solution of a cracked rod (Ref. 4) gave similar results. The measured value of K_I = 0.57±0.03 MPa√m is similar to that of the other highly alloyed glasses (Ref. 5) shown in Table 2 (0.50 to 0.75 MPa√m in air).

Slow Crack Growth

Slow crack growth properties were measured by method ASTM International C1368 with the exception of the specimen used: instead of standard beams or disks, funnels were tested by applying a bending moment via loading at the edge of the funnel mouth, thereby allowing the inherent crack growth mechanisms to be exhibited. Failure typically occurred in the abraded region of the funnel stem, as shown in Figure 11. The symmetry and cantilever curl exhibited on the fracture surface imply that simple bending was achieved in the tests, Figure 11(c). The resultant fracture strength is shown in Figure 12 and the crack velocity curves are shown in Figure 13 for the power and exponential functions, given respectively as

$$v = \frac{da}{dt} = A_1 K_I^{n_1} = A_1^* \left[\frac{K_I}{K_{IC}} \right]^{n_1} \tag{3}$$

and

$$v = \frac{da}{dt} = A_2 \exp\left(n_2 K_I\right) = A_2 \exp\left(n_2^* \frac{K_I}{K_{Ic}} \right) \tag{4}$$

where v, a, and t are crack velocity, crack size, and time, respectively. Constants A and n are the material/environment dependent SCG parameters, and K_I and K_{IC} are, respectively, the Mode I stress intensity factor and the critical stress intensity factor or fracture toughness. The parameters are summarized in Table 3. The MOMA glass exhibits similar cracks growth parameters as Corning 0120, another high lead glass.

All of the funnel test specimens used to estimate SCG parameters failed in the abraded region of the constant moment section. However, it is noteworthy that during testing in air, several specimens failed at low stress due to large, spurious flaws located in the metallized section of the spout. When testing in dry nitrogen, the problem was exacerbated and failure frequently occurred in the metallized region. The spurious flaws can only be eliminated via inspection or proof testing.

Summary

The strength, fracture toughness, slow crack growth parameters and Young's modulus of a high lead glass were measured. The high lead glass exhibits lower fracture toughness and is more susceptible to slow crack growth than soda-lime silicate. In general, glasses modified with oxides such as PbO and BaO exhibit lower fracture toughness and are more susceptible to stress corrosion than high purity glasses such as fused silica (n = 40) (Ref. 5).

References

1. S.W. Freiman, T.L. Baker, and J.B. Wachtman, Jr. "A Computerized Fracture Mechanics Database for Oxide Glasses," NBS Technical Note 1212 (National Bureau of Standards, 1985).
2. M. Khanisanij and H. Abdul Aziz Sidek, "Elastic Behavior of Borate Glasses Containing Lead and Bismuth Oxides," Advances in Materials Science and Engineering Volume 2014, Article ID 452830.
3. J.C. Newman and I.S. Raju, "An Empirical Stress Intensity Factor Equation for the Surface Crack," Engineering Fracture Mechanics 15 [1-2] 1981, pp. 185-192.
4. Y. Murakami and H. Tsuru, "Stress-Intensity Factor Equations for a Semi-Elliptical Surface Crack in a Shaft under Bending," Stress Intensity Factors Handbook, Soc. Mater. Sci., Japan, (1986).
5. J. Salem and R. Tandon, "Test Method Variability in Slow Crack Growth Properties of Sealing Glasses," *International Journal of Fatigue*, 32, 557-564 (March 2010).

TABLE 1.—STRENGTH STATISTICS OF SPIRAL TUBES

Failure location	Number tested	Average S_f (MPa)	Standard deviation	CV, percent	Weibull m	σ_θ MPa
All	40	61.3	5.3	9	14.1	63.5
Unabraded	6	61.1	8.0	13	10.6	74.5
Metallized	6	61.6	5.2	8	14.0	71.5
Abraded	28	61.2	4.9	8	14.8	64.8

TABLE 2.—FRACTURE TOUGHNESS (MPa√m) OF GLASSES (REF. 5)

Material	Environment	
	Air (%RH/°F)	Dry N_2
MOMA	0.57±0.03 (30/74)	0.69±0.01
Corning 0120	0.50±0.02 (34/76)	0.67±0.02
Electro-Glass 2164	0.61±0.05 (32/73)	0.74±0.03
Schott S8061	0.64±0.01 (23/73)	0.72±0.02
Schott S8070	1.57±0.03 (60/73)	1.90±0.03
Schott 8330	0.61±0.04 (60/73)	0.72±0.04
Soda lime silicate	0.75±0.04 (35/73)	0.80±0.01
Ba-doped	0.72±0.002 (23/73)	0.76±0.01
Silica, 7980	0.73±0.04 (45/75)	0.77±0.02

TABLE 3.—SUMMARY OF SLOW CRACK GROWTH (SCG) PARAMETERS FOR GLASSES (REF. 5)

Material and relative humidity	n	B $MPa^2 \cdot s$	A m/s $(MPa\sqrt{m})^{-n}$	n_2 $(MPa\sqrt{m})^{-n}$	A_2 m/s	# Tested
MOMA, 30% RH	19.5±2.1	2.5	$1.9\times10^{+1}$	51.5	2.3×10^{-16}	25
0120, 95% RH	17.0±3.1	0.6	$2.4\times10^{+1}$	49.2	5.3×10^{-15}	36
0120, 2% RH	23.2±5.3	4.3	$2.8\times10^{+1}$	61.1	4.2×10^{-19}	30
2164, 95% RH	12.9±1.1	6	2.3×10^{-1}	36.7	1.7×10^{-13}	65
2164, 2% RH	22.1±3.9	39	3.0×10^{-1}	36.6	1.7×10^{-16}	48
S8070, 95% RH	19.8±2.6	60	4.9×10^{-9}	16.1	3.9×10^{-16}	25
S8070, 2% RH	25.0±3.9	3,079	2.6×10^{-12}	17.1	2.8×10^{-19}	25
8330, 95% RH	17.1±1.3	5	5.6×10^{-1}	40.8	6.4×10^{-15}	25
8330, 3% RH	24.5±3.9	19	8.0×10^{-1}	38.1	1.6×10^{-16}	30
8330, 1% RH	30.0±3.6	2,855	2.1×10^{-2}	38.3	1.8×10^{-18}	30
Soda Lime Silicate, H_2O	20.1±0.9	5	7.5×10^{-1}	45.1	8.6×10^{-17}	30
7980, Fused Silica, H_2O	39.3±3.2	0.00013	$1.1\times10^{+7}$	88.3	1.2×10^{-24}	50

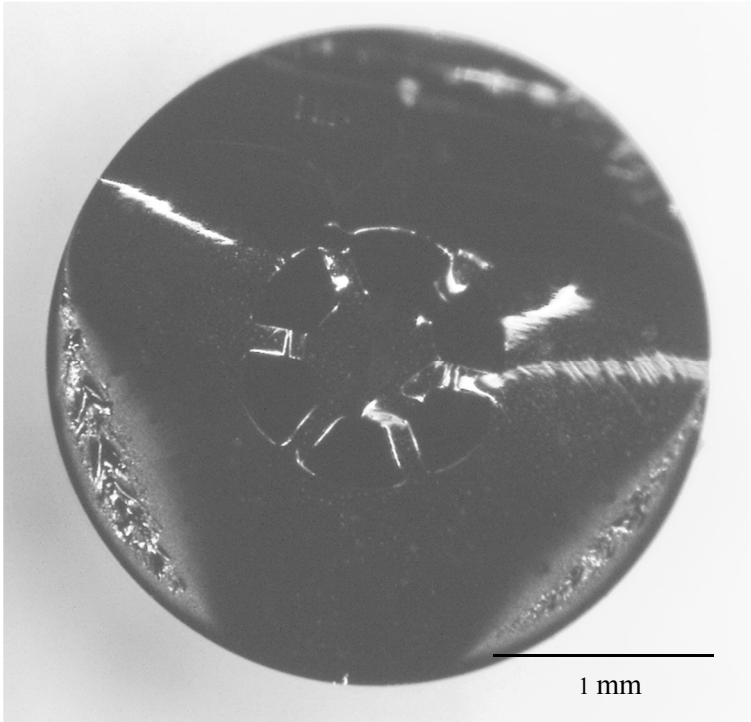

Figure 1.—Fracture cross section of strength test specimens.

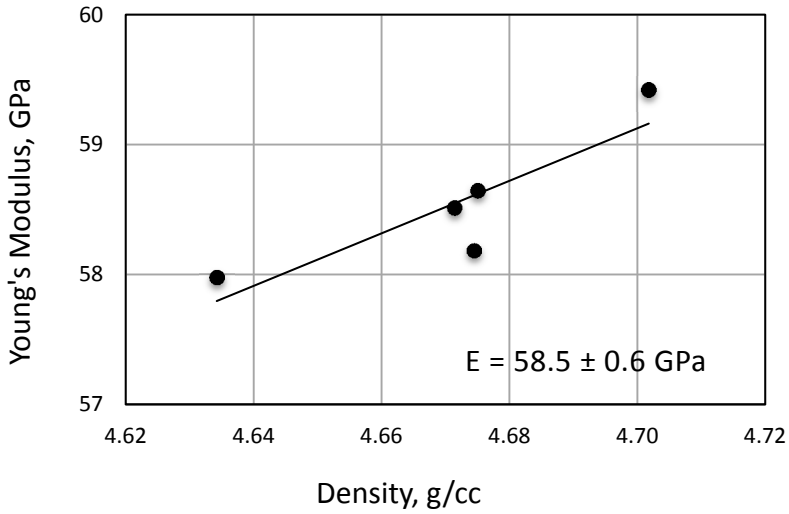

Figure 2.—Dyanmic modulus and density.

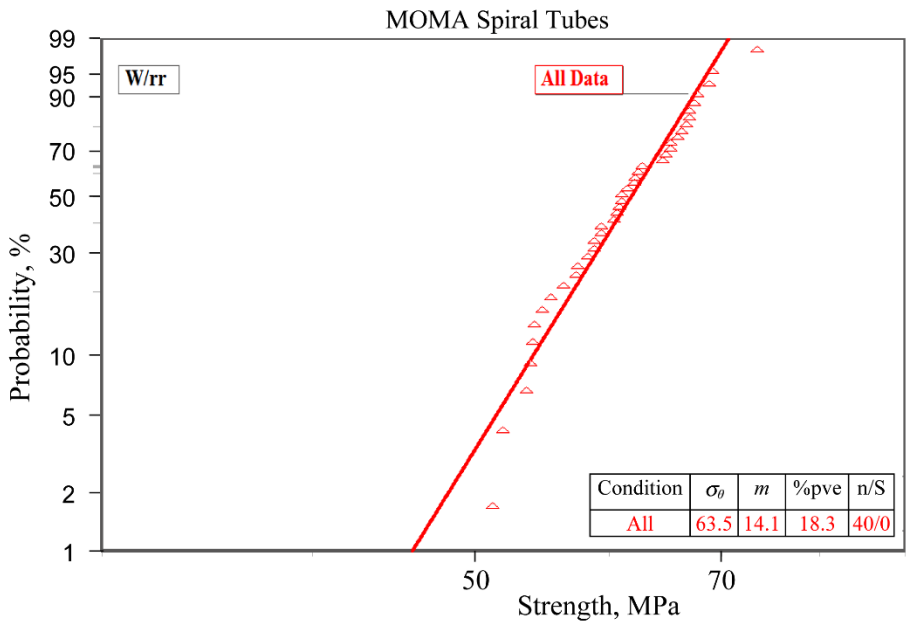

Figure 3.—Weibull distribution for all the data, as determined with rank regression.

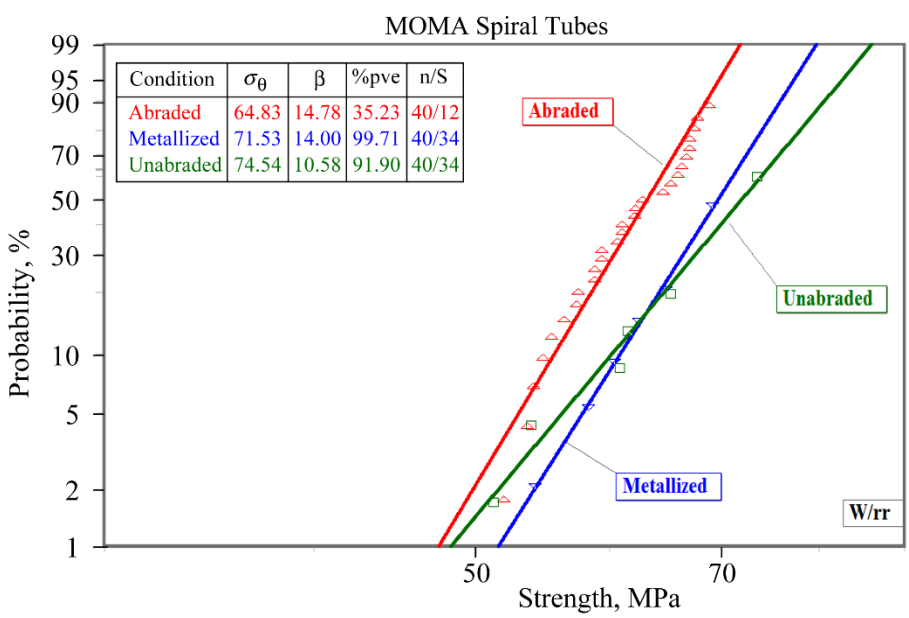

Figure 4.—Weibull distributions censored by fracture location.

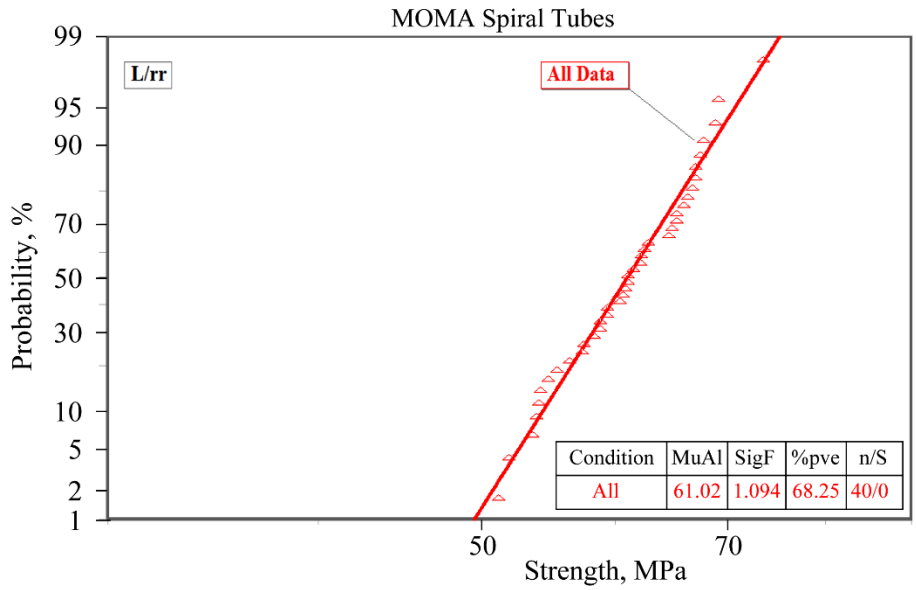

Figure 5.—Log normal distribution for all the data.

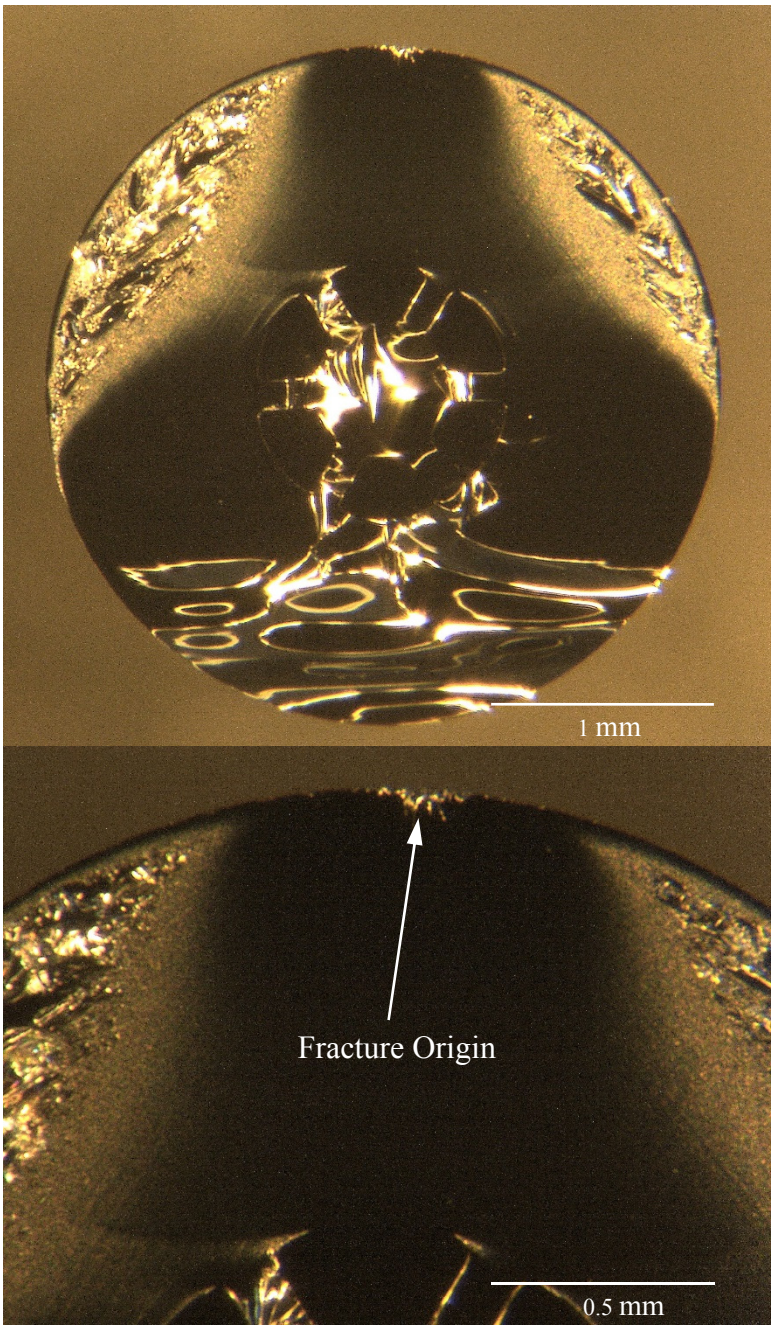

Figure 6.—Fracture origin in SN – 0035.

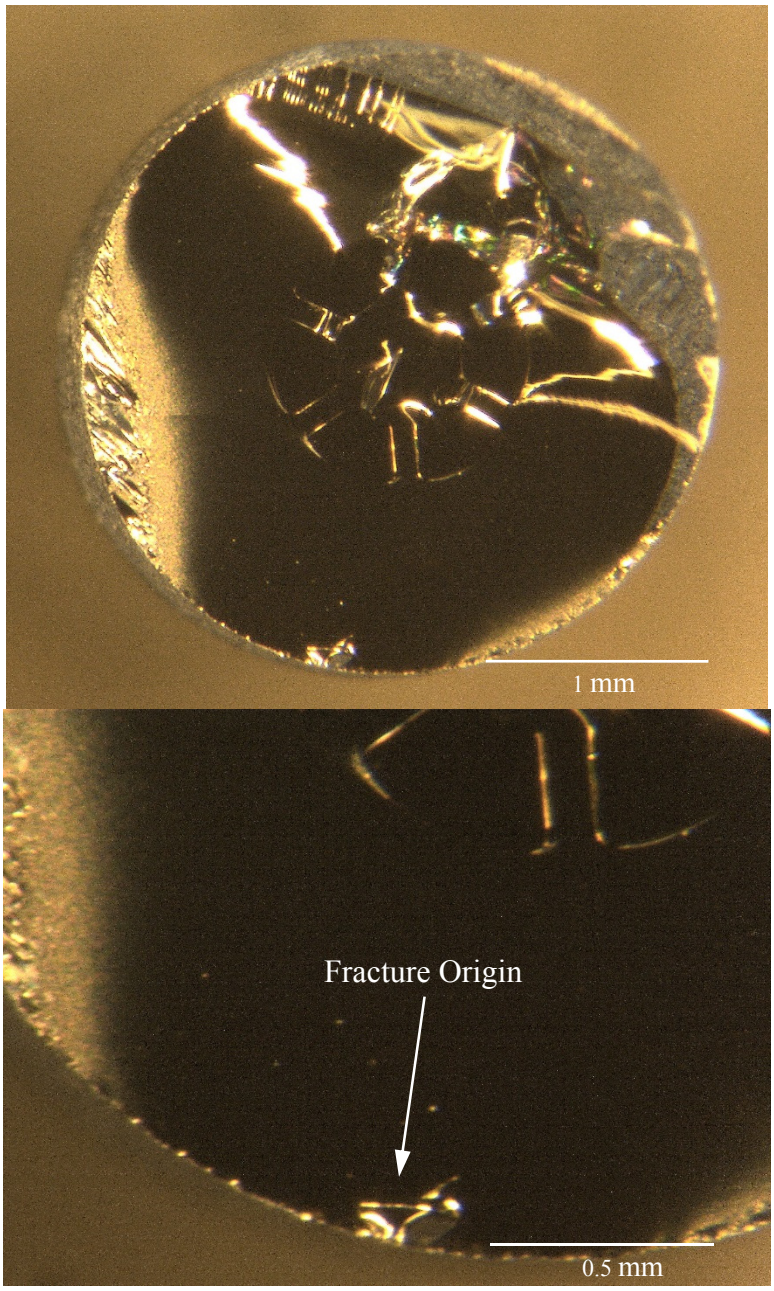

Figure 7.—Fracture origin in SN – 0039.

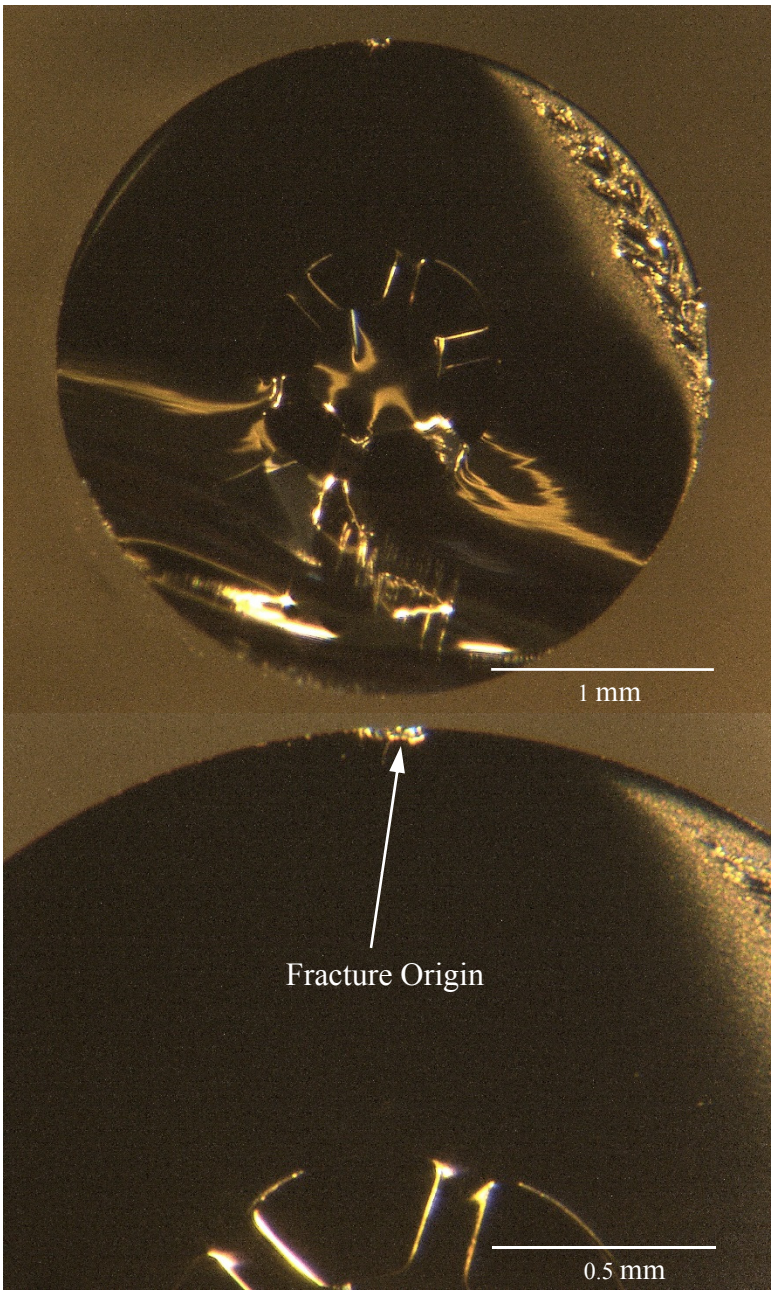

Figure 8.—Fracture origin in SN – 0040.

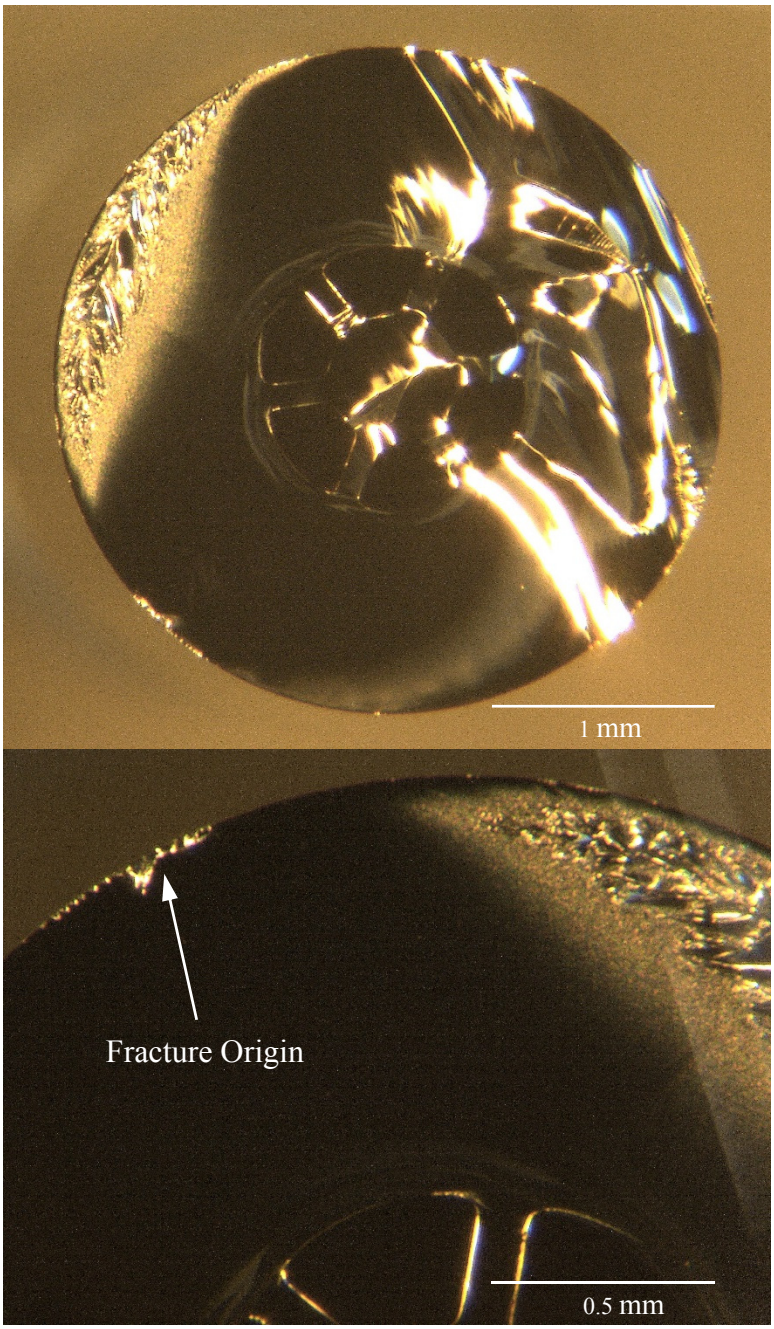

Figure 9.—Fracture origin in SN – 0031.

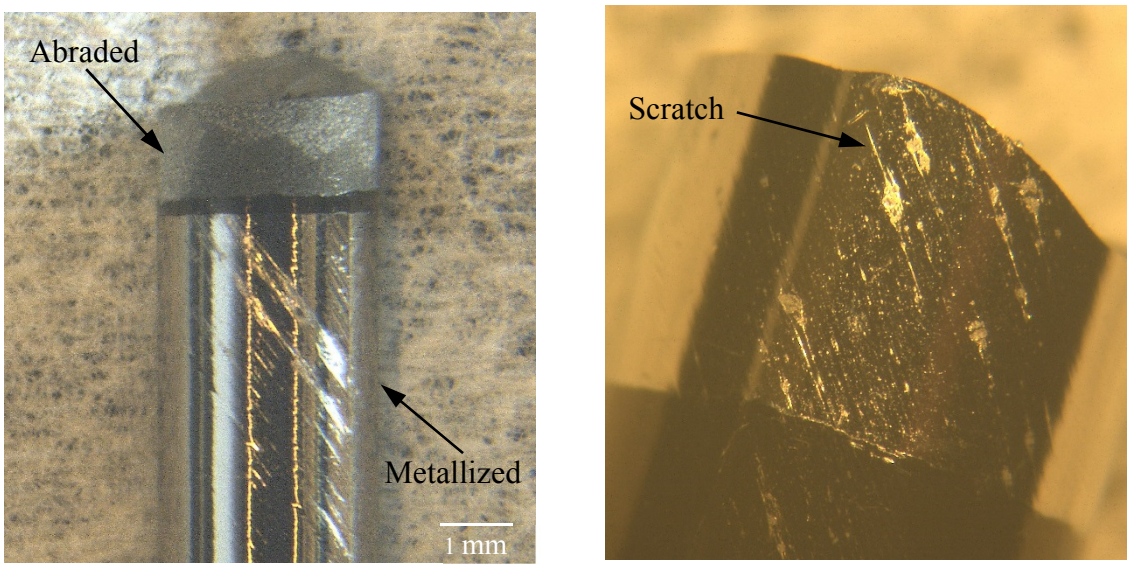

Figure 10.—Surface damage on tubular strength test specimens.

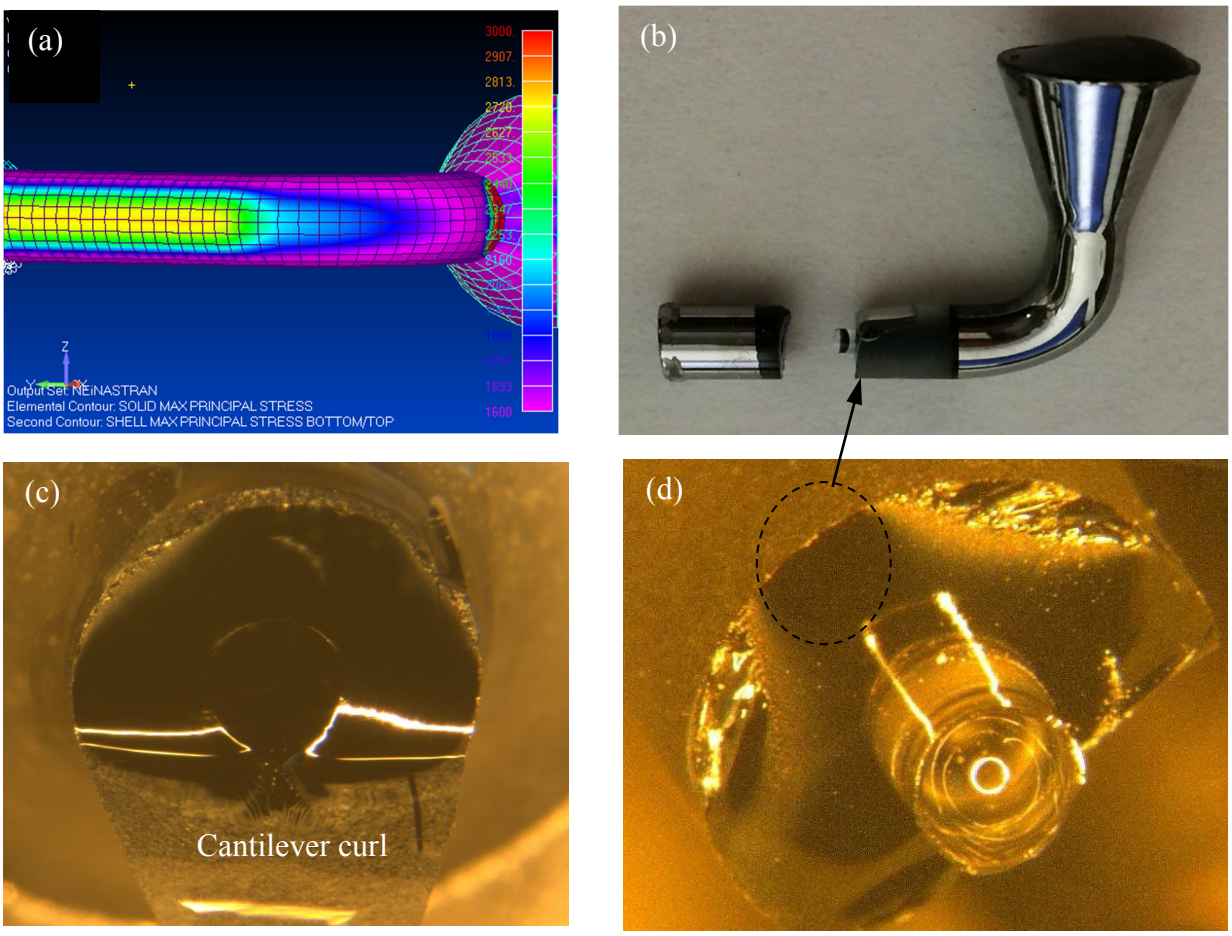

Figure 11.—Slow crack growth test specimen: (a) finite element analysis of test configuration, (b) fractured test specimen, and (c) and (d) fracture surfaces.

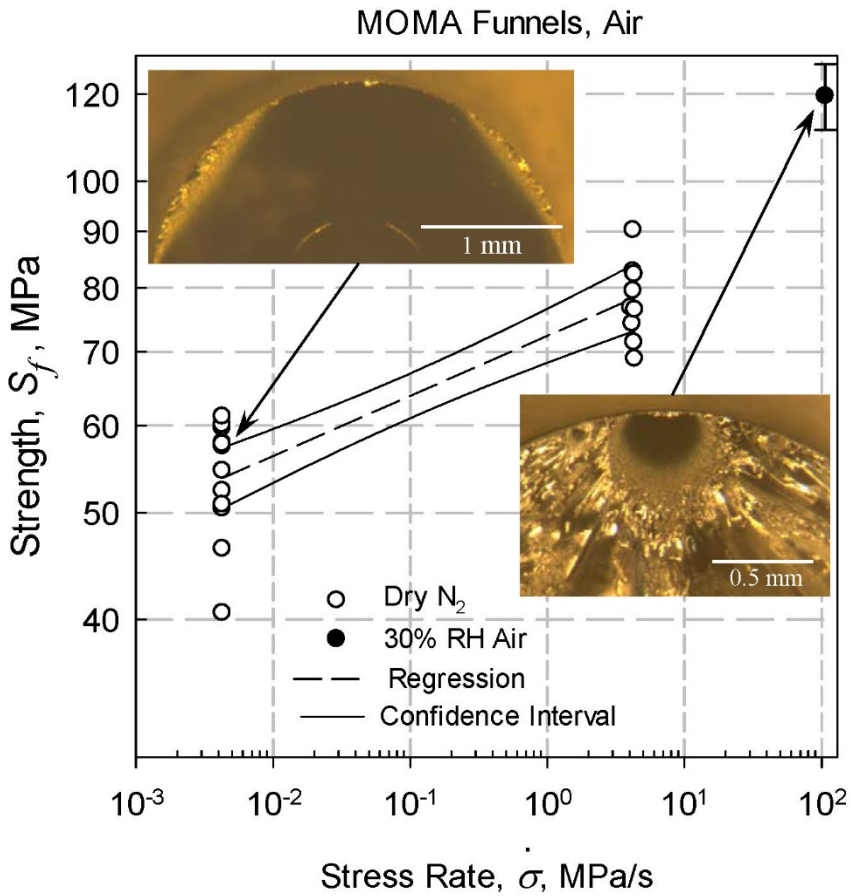

Figure 12.—Fracture strength as function of stress rate. Insets show typical fracture mirrors.

(a)

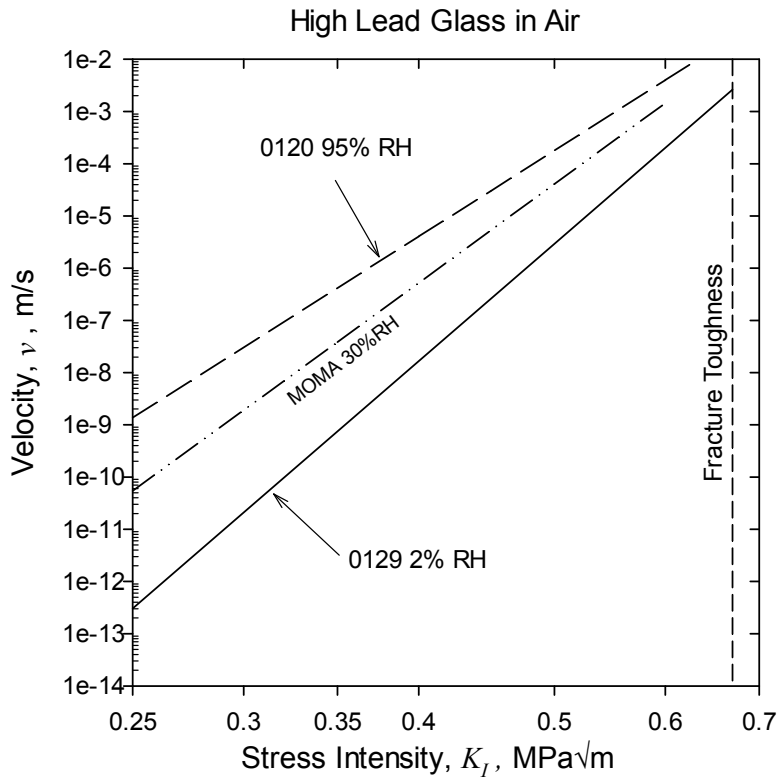

(b)

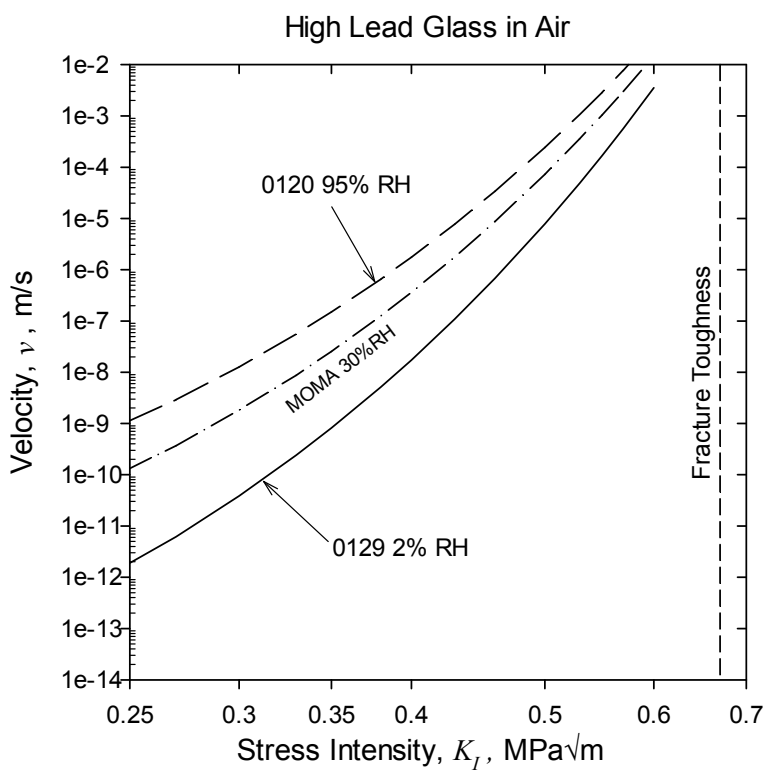

Figure 13.—Crack velocity of high lead glasses as a function of stress intensity for (a) power law and (b) for the exponential law.